Pursuant to the DOE Public Access Plan, this document represents the authors' peer-reviewed, accepted manuscript.
The published version of the article is available from the relevant publisher.

THE JOURNAL OF PHYSICAL CHEMISTRY C
A JOURNAL OF THE AMERICAN CHEMICAL SOCIETY

pubs.acs.org/JPCC

Perspective

Water and Solute Activities Regulate CO_2 Reduction in Gas-Diffusion Electrodes

Nathan T. Nesbitt* and Wilson A. Smith*

Cite This: https://doi.org/10.1021/acs.jpcc.1c01923

Read Online

ACCESS | Metrics & More | Article Recommendations | Supporting Information

ABSTRACT: Electrolysis of CO_2 at gas-diffusion electrodes (GDEs) has typically been limited by the supply of gas to the electrocatalyst, overshadowing the importance of the supply of water. However, at high current densities that approach 1 A cm^{-2}, where the electrolyte becomes highly concentrated in the catalyst layer of a GDE, the activity of water and solutes deviate from their bulk dilute solution values, potentially slowing reaction rates and changing reaction equilibrium potentials. In addition, as flow plates for the gas stream are introduced to enable larger electrodes and high single pass conversion of CO_2 to product, variations in the gas composition will become important. By drawing upon literature for the oxygen reduction reaction (ORR), here we explain how to account for these effects in future modeling and experimental work, with particular attention to accurate use of the Nernst equation for electrode potentials and the Arrhenius equation for reaction rates. Specifically, using measurements of KOH solvent and solute activity reported in literature, and assuming the second protonation of CO_2 by water as the rate-determining step, we show the Nernst equation dilute-solution approximation of the CO_2 to CO equilibrium potential to be accurate below 5 M KOH, but it has a 74 mV error when increasing the concentration up to 10 M KOH. Finally, a simple one-dimensional model of a serpentine flow-field on a GDE demonstrated that a reactor with constant pressure of 1 bar and 1 A cm^{-2} at the inlet had only ~0.3 A cm^{-2} at the outlet for a conversion in CO_2 partial pressure from 0.90 to 0.48 bar, showing the significant practical implications of this work.

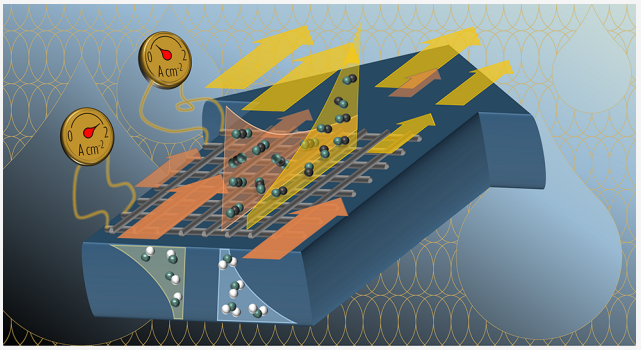

Downloaded via NATL RENEWABLE ENERGY LABORATORY on June 2, 2021 at 17:32:15 (UTC).
See https://pubs.acs.org/sharingguidelines for options on how to legitimately share published articles.

INTRODUCTION

Background. Electrochemical CO_2 reduction (CO_2R) is a rapidly developing technology that, if successfully commercialized, may provide a means to produce fuels and commodity chemical feedstocks with renewable energy, rather than from fossil fuels. CO_2R was originally performed in so-called aqueous H-cells, which had the cathode fully immersed in a liquid electrolyte and CO_2 supplied to the cathode by dissolution into the electrolyte. Subsequently, current densities over 10× higher were achieved by using reactors with gas-diffusion electrode (GDE) cathodes.[1] GDEs position the interface of gas-phase CO_2 and liquid electrolyte in close proximity to the catalyst layer (CL), providing fast diffusion of CO_2 in the gas-phase, as well as fast diffusion across mere tens to thousands of nanometers of liquid between the gas-phase and the electrocatalyst. Here, the term GDE is as defined by recent CO_2R studies that, using the GDE architecture, have been able to increase operational current densities to near and above 1 A cm^{-2}.[2−7]

The high performance of GDE devices has emphasized the importance of a plentiful supply of CO_2 via a facile diffusion pathway. This has encouraged a CO_2-centric perspective on assessing and improving CO_2R GDE performance. Here, we give an in-depth explanation of the role of water in a CO_2R GDE, in particular how water and solute activities likely regulate CO_2R activity and equilibrium potentials in the CL and what further computational and experimental work is needed to understand and further optimize the activity of this important chemical reaction.

Current Status. The transition of the CO_2R research field to GDE-based architectures has been growing significantly over the past several years. Modeling has kept apace by simulating different water, ionomer, and catalyst distributions in the CL of the GDEs,[8−16] predicting the corresponding CO_2 and current distributions and predicting water activity for membrane electrode assemblies primarily hydrated by water vapor. Further work has assessed the effect of water flooding in the GDE, a common mode for GDE deactivation during long duration stability tests.[17,18] These advances have moved the field toward more stable GDEs, with control over water distribution in the

Received: March 3, 2021
Revised: April 23, 2021

© XXXX American Chemical Society

Pursuant to the DOE Public Access Plan, this document represents the authors' peer-reviewed, accepted manuscript.
The published version of the article is available from the relevant publisher.

GDE to ensure robust pathways for CO_2 to diffuse and react with protons and electrons at catalytic active sites.

Importantly, modeling[8] and experiments[19] have shown that high current densities produce large quantities of OH^-, which attracts cations and causes elevated concentration and pH of electrolyte in the CL. This elevated electrolyte concentration and pH cause faster conversion of CO_2 into (bi)carbonate, diminishing the CO_2 supply to the CL and increasing electrolyte viscosity, slowing CO_2 diffusion to the CL. The elevated concentrations increase ion density and thereby electrolyte conductivity until they reach 5 molar (M) for NaOH and 7 M for KOH, above which high viscosity lowers the conductivity.[20] Concentrated (5−7 M) KOH electrolytes have also been used intentionally to suppress HER and optimize electrolyte conductivity;[4] however, this comes at the cost of low energy efficiency due to CO_2 conversion to (bi)carbonate[21,22] and, as discussed below, may introduce undesirable changes to water and solute activities.

In one example of the importance of water supply to the CL, by increasing the stirring of the bulk electrolyte, the CL electrolyte concentration was lowered, allowing higher CO_2 concentrations in the CL.[8] In membrane electrode assemblies (MEAs), it was also demonstrated that the water supply, rather than CO_2 supply, limited the device current density.[9]

Another important parameter to incorporate into models and experiments is the water and solute activity at the catalyst surface. The high local electrolyte concentrations in the microenvironment of the CL lowers water activity and increases solute activity, slowing the CO_2R reaction rate and changing reaction equilibrium potentials. These effects have been commented on in recent modeling literature,[14] but have yet to be directly accounted for in experimental design or modeling work. In recent studies on PtO reduction and the oxygen reduction reaction (ORR), however, the phenomena have been explicitly shown.[24−26] In the following sections, we explore these effects in detail.

METHODS

Fitting Water Activity and Solute Activity Coefficients. The polynomial fits of water and solute activities of NaOH and KOH versus molarity were made with a script in Julia using the LsqFit and Polynomial packages. Activities and activity coefficients were obtained from least-squares fit coefficients tabulated for 25 °C in relevant literature.[27,28] Measurements from literature of molality and molarity of NaOH and KOH were used for conversion of data from a molal basis to molar basis.[29]

1D Modeling of Serpentine Flow Field. The 1D model was calculated with a script in Julia using the DelimitedFiles, Statistics, LsqFit, and Polynomials packages. Recursive formulas were used to calculate the CO_2 and CO partial pressures, the equilibrium potential of the CO_2R to CO reaction, and the current density at each position along the reactor flow field. The relevant equations and initial conditions are summarized in Table 1.

Table 1. 1D Model Parameters, Initial Conditions, and Equations

description	definition	symbol
	model parameters	
gas channel height	100×10^{-6} m	y_{gas}
gas channel width	100×10^{-6} m	z_{gas}
gas channel length	1 m	x_{gas}
gas channel length segment	10×10^{-6} m	x_{seg}
electrolyte	1 M KOH	c
gas flow rate	1.67×10^{-7} m^3 s^{-1} (10 mL min^{-1})	v_{gas_flow}
total gas pressure	1 bar	P_{total}
rate constant[8]	2.44×10^{-8} $moles_{CO}$ s^{-1} m^{-2}	$k^0_{CO_2}$
applied cathode potentials	−1.797 V vs SHE for 2 A cm^{-2} −1.757 V vs SHE for 1 A cm^{-2}	$E_{applied}$
standard potential	−0.933 V vs SHE	$E^{0,\ alkaline}_{CO_2/CO}$
symmetry factor	0.44	$\propto_c$
Faraday constant	96 485 C mol^{-1}	F
gas constant	8.314 J mol^{-1} K^{-1}	R
temperature	298 K	T
	initial conditions	
inlet partial pressure CO_2	0.9 bar	$p_{CO_2_in}$
inlet partial pressure CO	0.1 bar	p_{CO_in}
	model equations	
gas segment volume	$x_{seg} \times y_{gas} \times z_{gas}$ [m^3]	V_{seg}
time of gas segment over GDE segment	V_{seg}/v_{gas_flow} [s]	t_{seg}
partial pressure CO_2	$P_{total} - p_{CO}$ [bar]	p_{CO_2}
thermodynamic constant	F/RT [V^{-1}]	f
GDE segment area	$x_{seg} \times y_{gas}$ [m^2]	A_{CL_seg}
equilibrium potential	eq 8 [V vs SHE]	$E_{CO_2/CO}$
overpotential	$E_{applied} - E_{CO_2/CO}$ [V]	η
current density	eq 14 [A m^{-2}]	j
rate expression	eq 17 [$mole_{CO}$ s^{-1} m^{-2}]	r_{COER}
conversion of CO_2 to CO at a channel segment	$r_{COER} \times A_{CL_seg} \times t_{seg}$ [mole]	$\Delta_{CO_2 \rightarrow CO}$

RESULTS AND DISCUSSION

The following subsections discuss the existing experimental and modeling work that demonstrate how water and solute activity affect electrochemical reactions, at what electrolyte concentrations and electrode conditions the effect is non-negligible, and what further work is needed to better understand CO_2R in GDE and MEA architectures.

Water and Solute Activities' Effect on Reaction Equilibrium Potential. Here, we give a detailed overview of how water and solute activity are defined and measured and their influence on the equilibrium potential of electrochemical reactions.

The activity of water represents the availability of water molecules for chemical/physical interactions, such as to hydrate ions in solution, evaporate into the headspace of a vessel, or participate in electrochemical reactions. The water activity ranges from 0 to 1, equal to unity when the water is pure. At low solute concentrations, the activity of water (a_{H_2O}) can be approximated by the partial pressure of water vapor above the solution (p_q) divided by the partial pressure of water vapor above pure water (p_0), $a_{H_2O} = p_q/p_0$. At higher concentrations, a more complicated expression is necessary,[28,30,31] but it is still derived from the thermodynamic definition of activity, $a_q = e^{\mu_q - \mu^\theta_q/RT}$, where μ_q is the chemical potential of the species q in the condition of interest, μ^θ_q is the chemical potential of the species q in a defined standard state, R is the gas constant, and T is the absolute temperature.

For water activity, the commonly used standard state is pure water. Figure 1a shows the measured water activity as a function

https://doi.org/10.1021/acs.jpcc.1c01923
J. Phys. Chem. C XXXX, XXX, XXX−XXX

Pursuant to the DOE Public Access Plan, this document represents the authors' peer-reviewed, accepted manuscript.
The published version of the article is available from the relevant publisher.

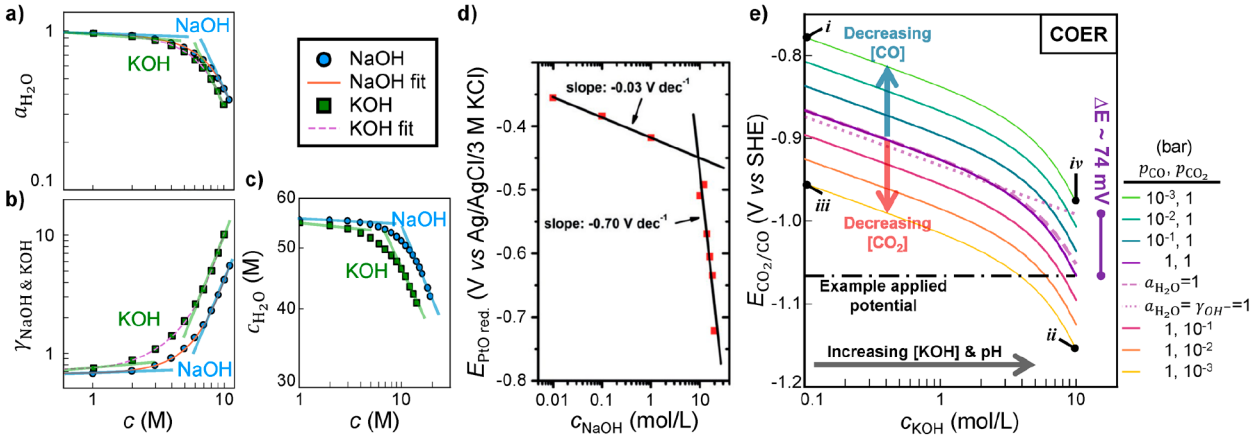

Figure 1. Dependence of (a) solvent activity, (b) solute activity, and (c) solvent molarity on KOH molarity in aqueous solutions. (d) Dependence of PtO/Pt equilibrium potential on NaOH molarity. (e) Dependence of CO_2/CO equilibrium potential on KOH molarity, CO_2 molarity, and CO molarity. Panel d adapted with permission from ref 24. Copyright 2018 Wiley VCH.

of solute concentration for aqueous solutions of KOH and NaOH, common electrolytes for CO_2R and the oxygen reduction reaction (ORR), respectively. At high solute concentrations, the water activity can drop significantly to below 0.5 for KOH concentrations above 8 M and NaOH concentration above 9 M. While water activity is typically reported against molality (moles of solute per kilogram of solvent) to avoid a temperature dependence, here it has been converted to molarity[29] (moles of solute per liter of solution) for the convenience of the CO_2R research field, which typically uses molarities; we use the variable c and unit M to indicate concentrations in molarity.

Solute activity uses a different common choice of standard state to define activity. For dissolved solids and liquids the standard state is a concentration of 1 M, and the activity coefficient goes to one at infinite dilution. Consequently, the activity for a solid or liquid solute is commonly defined with an activity coefficient (γ_q) and the ratio between a concentration of interest (c_q) and the standard 1 M concentration (c_q^0), giving $a_q = \gamma_q(c_q/c_q^0)$ for a given solute q. Figure 1b shows the activity coefficient for the respective solutes Na^+, K^+, and OH^- of various aqueous solutions of NaOH and KOH. For dissolved gases, a similar convention is used, but with concentration defined by the associated partial pressure (p_q) and the standard state at 1 bar partial pressure (p_q^0), giving activity as $a_q = \gamma_q(p_q/p_q^0)$; Appendix A shows the derivation of the activity coefficient for dissolved gas (see Supporting Information, for Appendices A–H). Unlike the simple monotonic decrease in water activity with increasing solute concentration, the solute activity is nonmonotonic. The ratio c_q/c_q^0 or p_q/p_q^0 just equals the solute molarity or partial pressure given the standard states defined above, but the activity coefficient is more complicated. As shown in Figures S7–S12, the activity coefficient equals 1 at very dilute concentrations, drops below 1 as it approaches 1 M, and then increases, reaching 4.2 by 10 M NaOH and reaching 10.4 by 10 M KOH.

In addition to temperature independence, there is another reason that molality is convenient to use when considering high solute concentrations. By its definition, the molality of a solvent cannot change with thermodynamic or process parameters. While much research in electrochemistry uses sufficiently dilute solutions to assume the molarity of water does not change with varying solute concentration, we will see this is not the case for the high electrolyte concentrations in GDE CLs operating at high current densities. As shown in Figure 1c and Figures S3–S6, the molarity of water drops ~10% to 50 M by 7 M KOH or 12 M NaOH.

Many models have been developed to express the activity of water and activity coefficients of solutes in concentrated salt solutions. Lewis et al. was the first,[32] followed by Debye and Huckel who developed an equation to account for interaction-attraction effects of species in solution.[31,33] Pitzer[34] proposed a modified Debye–Huckel equation that included empirical expressions for the second and third virial coefficients. These coefficients, sometimes with modifications to the equation, have been tabulated for a variety of solution species.[31]

To improve ease-of-use of water and solute activities for the researchers in the CO_2R field, we have provided polynomial fit coefficients for water and solute activity vs molarity in Table S1. These fits are plotted as solid red and dashed magenta lines, respectively, in parts a and b of Figure 1. Plots of the fits against a wider range of molarity and against molality are provided in Figures S3–S19.

To give a clearer demonstration of the effect of water activity on electrochemical reactions, before discussing the more complicated CO_2R, we first discuss the solid reactant/product pair Pt/PtO at a scanning electrochemical microscope (SECM) probe in different NaOH concentrations. The expected reaction is,

$$PtO + H_2O + 2e^- \rightarrow Pt + 2OH^- \quad (1)$$

which, assuming unit activity for solids and applying the Nernst equation, has the potential dependence on water and OH^- activity,[24]

$$E_{PtO/Pt} = E^0 + \frac{RT}{nF} \ln \frac{a_{H_2O}}{a_{OH^-}^2} \quad (2)$$

where n is the number of electrons per PtO molecule, R the gas constant, and T the absolute temperature.

Figure 1d shows the measured peak potential of PtO reduction, $E_{PtO\ red.}$, from cyclic voltammograms recorded in various NaOH concentrations. This is used as an approximation for $E_{PtO/Pt}$. Being defined by a standard state of 1 M OH^-, the OH^- activity should increase along with NaOH concentration. Water activity, on the other hand, defined by the standard state of pure water, will decrease with increasing NaOH concen-

https://doi.org/10.1021/acs.jpcc.1c01923
J. Phys. Chem. C XXXX, XXX, XXX–XXX

Pursuant to the DOE Public Access Plan, this document represents the authors' peer-reviewed, accepted manuscript.
The published version of the article is available from the relevant publisher.

tration. The ratio of these activities determines $E_{PtO\ red.}$, and the semilog plot in Figure 1d thus shows the rate of change of this ratio with increasing NaOH molarity. A change in slope at ~10 M NaOH suggests this is a critical concentration for this electrochemical reaction, above which $E_{PtO\ red.}$ is much more sensitive to the NaOH molarity. Figure 1a shows a change in slope of the log of water activity at ~5 M NaOH, and Figure 1b a change in slope of the log of NaOH activity coefficient also at ~5 M NaOH. This aligns roughly with the significantly different slopes below 1 M and above 10 M in Figure 1d. Equation B-5 in Appendix B shows the explicit relationship between the log−log plots of Figure 1a,b and the semilog plot of Figure 1d.

To establish an intuitive understanding of these phenomena, we make the following observations. The change in log of water activity and log of NaOH activity coefficient at ~5 M NaOH correlates with a drop by 2% of the molarity of water, and the molarity of water starts to decrease quickly as the NaOH molarity further increases. This indicates an insufficient supply of the water molecules present to hydrate the ions, preventing Na^+ and OH^- ions from filling "empty space" in the solution as they do at lower concentrations indicated by the water molarity beginning to diminish. Thus, H_2O molecules become unavailable for the desired electrochemical reactions, and the Na^+ and OH^- ions develop an outsized availability for reaction, resulting from a high activity coefficient. In this case, the effect of OH^- ions is to oppose the PtO reduction, i.e., to shift $E_{PtO\ red.}$ to more cathodic potentials.

Relating this to CO_2R, we see that the equilibrium potential for a reaction can be sensitive to solute and solvent activities, especially at high concentrations. Thus, for a GDE CL with uniform electric potential across the CL, gradients in electrolyte concentration across the CL would make gradients in reaction equilibrium potential. This would give a spatial distribution to the overpotential for each electrochemical reaction that is possible at the catalyst, which could have important implications for CO_2R selectivity. This adds a little commented on factor to the myriad factors affecting overpotential distribution, such as distributions in temperature and catalyst surface structure. The dependence of the equilibrium potential for the electrochemical conversion of CO_2 to CO, $E_{CO_2/CO}$, on solvent and solute activities can be determined by the reaction mechanism and rate-determining step (RDS).

As a relevant example for CO_2R, we consider nanostructured Ag catalysts, which are selective for the CO evolution reaction (COER) and offer reasonable comparisons to Cu and Au catalysts. To determine the rate-determining step (RDS) and thus the proper Nernst equation for $E_{CO_2/CO}$, we reference recent work on COER on nanostructured Ag catalysts.[35] Despite the study's use of neutral pH solutions containing a buffer electrolyte (e.g., 0.5 M NaHCO3, pH 7.2) and low overpotentials, where the Tafel slope is not obscured by mass transport of reactants or products, it is thorough and is the most relevant study to our system. In the proposed reaction mechanism, the first protonation was by the buffer anion HCO_3^- and the second protonation by H_2O; the second protonation was found to be the RDS. This gives the overall reaction of

$$CO_2 + HCO_3^- + H_2O + 2e^- \rightarrow CO + OH^- + CO_3^{2-} + H_2O \quad (3)$$

Broken down into sequential steps, this gives

$$CO_2 + HCO_3^- + e^- + * \rightarrow COOH_{ads} + CO_3^{2-} \quad (4.1)$$

$$COOH_{ads} + H_2O \xrightarrow[RDS]{} COOH_{ads}\cdots H^+ + OH^- \quad (4.2)$$

$$COOH_{ads}\cdots H^+ + e^- \rightarrow CO_{ads} + H_2O \quad (4.3)$$

$$CO_{ads} \rightarrow CO + * \quad (4.4)$$

The reported equilibrium potential for this reaction mechanism and RDS is[35]

$$E_{CO_2/CO} = E^{0,nano-Ag}_{CO_2/CO} + \frac{RT}{nF} \ln \frac{a_{CO_2} a_{HCO_3^-}}{a_{CO} a_{CO_3^{2-}} a_{OH^-}} \quad (5)$$

Cu and Au have shown a similar dependence on buffer anions for CO_2 protonation.[36−38] Further work would be necessary to confirm that this mechanism and RDS apply to COER at GDEs, at high current densities, and in concentrated alkaline electrolytes.

For alkaline electrolytes above pH 10 or 11, where the equilibrium ratio of HCO_3^- and CO_3^{2-} favors the latter, only H_2O would be available to protonate CO_2. Assuming H_2O for both protonation steps, but no change in the RDS for the Ag catalyst, would give an overall reaction of:

$$CO_2 + 2H_2O + 2e^- \rightarrow CO + 2OH^- + H_2O \quad (6)$$

Broken down into sequential steps gives

$$CO_2 + H_2O + e^- + * \rightarrow COOH_{ads} + OH^- \quad (7.1)$$

$$COOH_{ads} + H_2O \xrightarrow[RDS]{} COOH_{ads}\cdots H^+ + OH^- \quad (7.2)$$

$$COOH_{ads}\cdots H^+ + e^- \rightarrow CO_{ads} + H_2O \quad (7.3)$$

$$CO_{ads} \rightarrow CO + * \quad (7.4)$$

$E_{CO_2/CO}$ would then become:

$$E_{CO_2/CO} = E^{0,alkaline}_{CO_2/CO} + \frac{RT}{nF} \ln \frac{a_{CO_2} a_{H_2O}}{a_{CO} a_{OH^-}^2} \quad (8)$$

To validate this hypothesis, experiments that determine the Tafel slope and reaction order of CO_2R electrodes in alkaline electrolyte would need to be performed and compared with reaction mechanism calculations.[35] If the Tafel slope remained near 59 mV dec^{-1}, the reaction rate became independent of HCO_3^-, and the reaction order in OH^- became 2, then eq 6 would likely be valid.

The above explanation is particular to the assumed Ag surface and may not apply to many other catalysts. That said, this example of COER at a Ag catalyst demonstrates that gradients in activity (i.e., concentration) of CO_2, H_2O, CO, HCO_3^-, CO_3^{2-}, or OH^- could shift the equilibrium potential of CO evolution significantly. If this gradient was extended spatially along the flow channel over a CL, and the CL had a uniform applied potential (i.e., perfect conductor), then the overpotential for the reaction would vary spatially along the CL, as detailed in the following section.

Spatial Variation along Flow Channels of Reaction Equilibrium Potential. CO_2R literature[19,39] has, so far, typically cited the simplified Nernst equation to describe how $E_{CO_2/CO}$ changes with increasing $KHCO_3$ or KOH concentration. This equation depends only on pH and is usually written as

https://doi.org/10.1021/acs.jpcc.1c01923
J. Phys. Chem. C XXXX, XXX, XXX−XXX

Pursuant to the DOE Public Access Plan, this document represents the authors' peer-reviewed, accepted manuscript.
The published version of the article is available from the relevant publisher.

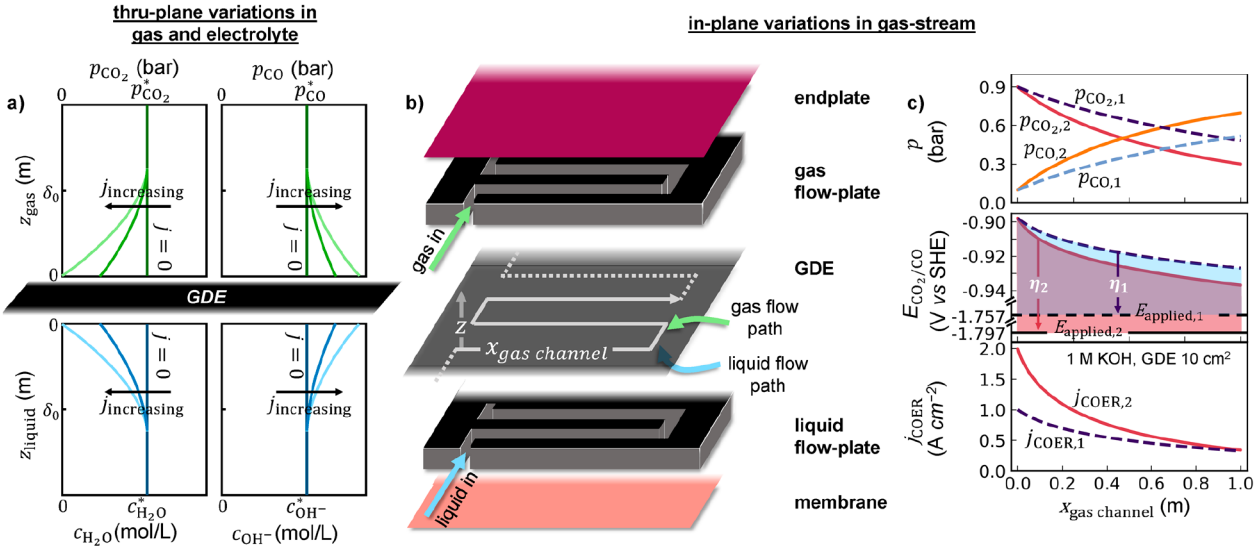

Figure 2. General trends of activity, concentration, and partial pressure gradients near a GDE CL. (a) (top) Schematic of gradient in partial pressure of CO_2 and CO vertically from the CL into the gas stream at three current densities; (bottom) schematic of gradient in concentration of H_2O and OH^- vertically from the CL into the electrolyte stream at three current densities. (b) Schematic of a GDE with serpentine flow fields above for gas and below for liquid, z represents thru-plane distance away from GDE surface (along surface normal), x represents in-plane distance along the flow path. (c) Plots from a simple 1D model of CO_2 and CO partial pressures, CO_2/CO equilibrium potential, and COER current density along parallel gas and liquid channels 1 m long.

$$E_{CO_2/CO} = -0.106 - 0.0591\text{pH} \quad (9)$$

This approximation is accurate for electrolyte concentrations with water activity and solute activity coefficients of 1. Notably, this is only accurate for acidic or neutral electrolytes, for which the overall reaction can be written:

$$CO_2 + 2H^+ + 2e^- \rightarrow CO + H_2O \quad (10)$$

For alkaline electrolytes, (per derivation in Appendix A, eqs A-7−A-15) the simplified Nernst equation is given by

$$E_{CO_2/CO} = -0.933 - 0.0591\text{pH} \quad (11)$$

In this case, the overall reaction is written:

$$CO_2 + H_2O + 2e^- \rightarrow CO + 2OH^- \quad (12)$$

Here we clarify a common misnomer in CO_2R literature. Since CO_2R was originally obtained only in acidic or neutral electrolytes, but is now often obtained in alkaline electrolytes, it has become common for manuscripts to write eqs 9 and 12 together, which is technically not accurate.

These simplified Nernst equations are special cases of eq 8. Figure 1e demonstrates the accuracy of the simplified Nernst equation for 0.1 to 10 M KOH. The dotted purple line shows the simplified Nernst equation (eq 11). The dashed purple line uses eq 8 and the experimental activity coefficient of KOH from Figure 1b, but with water activity still assumed to be 1. The solid purple line adds the effect of the water activity, using data from Figure 1a. The activity coefficients of CO_2 and CO are assumed to be 1, a valid assumption at standard temperature (298 K) for CO_2 below 2 mol % (i.e., below 1 M CO_2)[40] and CO below 4.8 M CO (see CO activity coefficient derivation in Appendix A, eqs A-1 to A-22, and Figure S3).[41−46] There are 20−50% variations in CO activity coefficient with changing temperature and electrolyte concentration and composition; consideration of these nuances lies outside the scope of this work, but could be worth future investigation. All purple lines have a ratio of $p_{CO_2}/p_{CO} = 1$.

From the purple lines in Figure 1e, the simplified Nernst equation is clearly quite accurate below 5 M KOH. At higher molarities, the simplified Nernst equation significantly underestimates the negative shift in $E_{CO_2/CO}$ with increasing molarity, reaching a ∼74 mV difference at 10 M between the simplified and activity dependent $E_{CO_2/CO}$.

To demonstrate the influence of the ratio p_{CO_2}/p_{CO} on $E_{CO_2/CO}$, CO_2 and CO partial pressures were each varied to 1, 10, and 100 mbar while the other was held at 1 bar. These lines are plotted in Figure 1e, and demonstrate a −30 mV shift in $E_{CO_2/CO}$ for each decade increase of p_{CO} or decade decrease in p_{CO_2}.

Figure 2a depicts the concentration gradient that develops vertically, through the plane of the GDE. With increasing current density, the reactant concentrations move toward zero and product concentrations move toward infinity at the CL surface. For an infinite bulk electrolyte or gas volume, the bulk partial pressures and concentrations will remain constant. Since $E_{CO_2/CO}$ is defined for the case of zero current density, eq 8 uses these bulk concentrations.

Figure 2b shows a GDE for COER with a serpentine flow pattern for gas and liquid streams. Such flow fields have been suggested for large electrode devices.[47−51] In this case, the bulk electrolyte and gas are not infinite, and they will vary in composition along the lateral flow path. At any given section of CL along this flow, the bulk concentrations for use in eq 8 are the result of upstream conversion of reactants to products. This implies that if one short segment of GDE along the flow field could be turned down to zero current while the rest continued running, the reactant and product concentrations from upstream in the flow would define the "zero current" electrolyte and gas composition of this small segment. Segmented cells, in which the cathode and/or anode are separated into arrays of individually electrically addressed sections, allow just such an experimental arrangement. They have also been used for hydrogen fuel cells to see variations in potential or current along flow fields for

https://doi.org/10.1021/acs.jpcc.1c01923
J. Phys. Chem. C XXXX, XXX, XXX−XXX

Pursuant to the DOE Public Access Plan, this document represents the authors' peer-reviewed, accepted manuscript.
The published version of the article is available from the relevant publisher.

different gas stoichiometries and flow rates[52,53] and would be interesting to see applied to CO_2R cathodes.

We can use Figure 1e to surmise variations in $E_{CO_2/CO}$ from hypothetical changes in electrolyte and gas stream composition in the flow field depicted in Figure 2b. For example, we consider a single-pass conversion of CO_2(g) to CO(g) in the gas stream high enough to cause a change from 1 bar CO_2 + 0.1 bar CO to 0.1 bar CO_2 + 1 bar CO in the dissolved gas of the CL. If a coflow (i.e., parallel flow) of electrolyte had an increase in CL electrolyte molarity from 0.1 M KOH to 10 M KOH, then $E_{CO_2/CO}$ would vary by 370 mV from inlet to outlet (the difference between annotations *i* and *ii* in Figure 1e). If, instead, the gas and liquid flows were in opposite directions (counterflows), then, with the same variations in composition of the gas stream and electrolyte, $E_{CO_2/CO}$ would vary by only 20 mV (difference between annotations *iii* and *iv* in Figure 1e). This suggests such counterflows could be quite advantageous for uniformity of current density in electrolyzers.

Figures 2b and 1e can also be interpreted from the perspective of overpotential, $\eta = E_{applied} - E_{CO_2/CO}$. For example, it is helpful to look at the case of the applied potential of −1.065 V vs SHE, shown as a horizontal black dash-dot line in Figure 1e. Assuming CO_2 and CO partial pressures in the gas flow are kept at partial pressures of 1 bar (Figure 1e purple lines), and the electrolyte at the inlet of a serpentine flow pattern was 0.1 M KOH, then $\eta \approx -200$ mV would be expected. If the electrolyte concentration at the outlet reached 10 M KOH due to the OH^- production from CO_2R, but the common assumption was made that $a_{H_2O} = 1$ and $\gamma_{OH^-} = 1$, then $\eta \approx -80$ mV would be expected. However, with accurate values of water and hydroxide activity used in eq 8, the 10 M KOH would actually have $\eta \approx 0$ mV.

To add a change in partial pressure of CO_2 and CO to the hypothetical situation above, in the condition of 10 M KOH in the CL with $\eta \approx 0$ mV, if p_{CO_2} was brought one decade below p_{CO} (a likely condition at the flow field outlet), this would cause $\eta \approx +30$ mV (i.e., the reverse of the desired reaction).

Understanding the dependence of $E_{CO_2/CO}$ on the local environment near a catalyst active site (referred to as the microenvironment) offers two advantageous opportunities. Electrolyzer design parameters, such as counterflows of gas and liquid, could help maintain uniform $E_{CO_2/CO}$ throughout the CL. On the other hand, variations in the microenvironment could provide an opportunity to benefit cascade reactions, where the product from one part of the CL is the reactant for another part of the CL (e.g., CO generated from CO_2R supporting ethylene production[54]).

Since increasing a product's partial pressure causes a negative shift in reaction potential, keeping a reactor saturated with a particular product could be a technique to prevent further production of that product, favoring a different one. For example, in a reactor designed to make CO for the purpose of producing syngas (a combination of CO and H_2), the H_2 from a water electrolyzer (or recycle loop) could be fed into the electrolyte of the CO reactor to prevent production of H_2 in the CO reactor. This would prevent a reactor optimized for CO production from in-efficiently producing H_2.

Water Activity Effect on Reaction Rate. This section discusses the effect of water activity and solute activity coefficients on reaction rate. The effect of water and solute activity on reaction rate has been previously described for the well-studied ORR, a good model reaction for COER since both consume water to produce OH^- and a gas product. The expected reaction is

$$O_2 + 2H_2O + 4e^- \rightarrow 4OH^- \tag{13}$$

with current I given by

$$I = -nFAr \tag{14}$$

where n is the moles of electrons consumed per mol of O_2 or CO_2, F the Faraday constant, A electrode area, and r reaction rate. The rate expression is[26]

$$r_{ORR} = k^0 a_{O_2} a_{H_2O}{}^2 e^{-\alpha_c f \eta} \tag{15}$$

where $f = F/RT$, and α_c is the cathodic charge transfer coefficient.

In experiments that supplied O_2 to the electrode via dissolution into the electrolyte at a gas−liquid boundary 0.1−1 μm from the electrode, the increasing NaOH concentration increased viscosity and decreased water activity; this slowed O_2 diffusion and decreased O_2 solubility, respectively, as demonstrated by oxygen depolarized electrodes (ODE) and scanning electrochemical microscopy (SECM) probes.[26,28,55,56] The limited O_2 mass transport slowed the ORR current in high concentrations of aqueous NaOH, such as 10 M.

In these studies, the decrease in O_2 diffusion and solubility caused by increasing NaOH concentration obscured the effect of H_2O activity on the ORR rate expression, shown in eq 15. Recent work circumvented this with a double-barrel nanopipette to supply O_2 locally to a Ag ORR catalyst.[25] The small separation between the O_2 source and Ag catalyst prevented solubility and viscosity from overshadowing the rate expression dependence on H_2O activity. In this arrangement (per Table S2) the current vs voltage measurements made in 0.1, 5, and 10 M NaOH showed a reaction order of 2 in H_2O ($I_{ORR} \sim a_{H_2O}{}^2$).

To relate these results from this ORR study to CO_2R, we consider, for example, the COER discussed above. Using the chemical reaction detailed in eqs 3 and 4, where bicarbonate provides the first protonation of CO_2 and the assumed RDS was the second protonation, the current I_{COER} is given by eq 14 and the rate expression,

$$r_{COER} = k^0 \frac{a_{CO_2} a_{H_2O} a_{HCO_3^-}}{a_{CO_3^{2-}}} e^{-\alpha_c f \eta} \tag{16}$$

Alternatively, for a more alkaline electrolyte, if the first protonation was from H_2O as detailed in eqs 6 and 7, but the RDS remained the second protonation, the current I_{COER} would be given by eq 14 and the rate expression,

$$r_{COER} = k^0 \frac{a_{CO_2} a_{H_2O}{}^2}{a_{OH^-}} e^{-\alpha_c f \eta} \tag{17}$$

The first case would have reaction order −1 for CO_3^{2-} and reaction order 1 for CO_2, H_2O, and HCO_3^-. The latter case would have reaction order −1 for OH^-, 1 for CO_2, and 2 for H_2O. In either case, the reaction rate would be diminished at low water activity and high OH^- activity. The HCO_3^- protonation case would be indirect for the neutral buffer electrolyte: increasing OH^- favors conversion of HCO_3^- into CO_3^{2-} and thus an increasing CO_3^{2-} concentration. This suggested lowering of hydroxide concentration also will mitigate CO_2 consumption by its conversion to bicarbonate and carbonate, important for energy efficiency of devices.[22]

https://doi.org/10.1021/acs.jpcc.1c01923
J. Phys. Chem. C XXXX, XXX, XXX−XXX

Pursuant to the DOE Public Access Plan, this document represents the authors' peer-reviewed, accepted manuscript.
The published version of the article is available from the relevant publisher.

The above dependence of $E_{CO_2/CO}$ and r_{COER} on the gas composition raises an important practical question: how does the current density vary along a flow field that is designed to achieve high single-pass conversion of CO_2 to CO? While clever cell design might mitigate gradients in H_2O, OH^-, and HCO_3^- activities, it is an explicit objective of COER reactors to achieve high single pass conversion of CO_2 to CO and thereby avoid the financial and energy cost of their separation. To answer this question, we used the reaction mechanism and RDS of eq 17 in a simple 1D model to calculate the change in gas composition, $E_{CO_2/CO}$, and j_{COER} along a serpentine flow field at a given applied potential and rate constant k^0.

The 1D model used a 1 m long channel with a $100 \times 100\ \mu m^2$ cross-section (total GDE geometric surface area 10 cm^2). For simplicity, the model assumed no thru-plane gradients in activities, concentrations, or partial pressures (i.e., the gas was assumed perfectly mixed in the vertical (z) direction); the gas was assumed dry and evaporation of electrolyte into the gas stream negligible; equilibration between anode and cathode was assumed ideal so that the electrolyte along the flow channel was a constant 1 M KOH; the GDE was assumed to be a perfect conductor so that the applied potential had no spatial variation along the channel. Equations, parameters, and initial conditions for this 1D model are summarized in Table 1.

The results of the model reveal profiles of p_{CO_2}, p_{CO}, $E_{CO_2/CO}$, and j_{COER} along the flow field channel, depicted in Figure 2c. For a reactor operating at either 2 or 1 A cm^{-2} at the inlet, the model showed a drop to ~0.3 A cm^{-2} at the outlet, a drop in η from −0.90 to −0.86 V for 2 A cm^{-2} (−0.86 to −0.83 V for 1 A cm^{-2}), and change in p_{CO_2} from 90% to 30% and p_{CO} from 10% to 70% for 2 A cm^{-2} (p_{CO_2} from 90% to 48% and p_{CO} from 10% to 52% for 1 A cm^{-2}). The effects of changing flow rate, gas channel width, and electrolyte concentration are depicted in Figures S21−S23.

The model results demonstrated that, due to the thermodynamic equilibrium that defines $E_{CO_2/CO}$ and the COER rate expression, a high conversion efficiency of CO_2 to CO necessitated a large variation in j_{COER} and η between the inlet and outlet of the reactor. Higher conversion efficiencies, which are desirable to avoid separation of CO_2 from CO, would have ever greater variations in j_{COER} and η.

The kinetic rate expression depended on the activities, concentrations, and partial pressures present at the CL during operation, not the bulk values as $E_{CO_2/CO}$ did. Thru-plane gradients depicted in Figure 2a would likely be large for GDE's operating at 1 or 2 A cm^{-2}, making our 1D model's assumption of no gradients a significant oversimplification. To model these thru-plane gradients would require 2D modeling of the gas and liquid flow channels, important future work to optimize high single-pass conversion CO_2R electrolyzers.[23] Measurement of these gradients would improve model accuracy and require probes with micrometer-scale thru-plane resolution, such as those for scanning electrochemical microscopy.[24]

Operando Study of ORR GDEs. Given the above effects of water and solute activity on electrochemical reactions and the possibility for a reduction reaction in a GDE to produce OH^- and alter the local electrolyte concentration, we now relate an operando study of an ORR GDE as a template for future CO_2R studies.

The GDE architecture used in the ORR study[26] assumed a narrow (80 nm thick) interface separating dry and flooded agglomerates in the GDE, and calculated the concentration of O_2 and various solutes as a function of distance into the flooded agglomerate region (from the gas−liquid interface). With no stirring of the bulk electrolyte, the dissolved O_2 concentration profile shrunk "almost to zero at the mass transport governed current density of $j_{ORR} = -1.26$ kA m^{-2}" (−126 mA cm^{-2}).[26] By stirring the electrolyte bulk, the accumulation of OH^- and Na^+ in the flooded agglomerate was diminished. These operating conditions kept the dissolved O_2 concentration profile from shrinking to zero by maintaining high water activity and low viscosity, which provided high O_2 solubility and fast O_2 diffusion, respectively.

To study the dynamics and kinetics of the system, the applied potential was stepped to a more cathodic potential, and the simulated and experimental j_{ORR} vs time response was compared. The results at these different potentials matched well and showed the time constant was "dominated by the mass transport of water and hydroxide ions between the reaction zone and the electrolyte bulk phase."[26] Thus, the current response was determined by water and OH^- mass transport, which was suggested to result from their effect on O_2 solubility and diffusion: upon increasing the applied potential, the current would spike but then settle over ~80 s as OH^- was generated, water activity decreased, viscosity increased, and O_2 supply decreased.

By observing the system's dynamic response, this study of the ORR was able to experimentally confirm the local electrolyte concentration in the GDE that was predicted by modeling. Specifically, for the particular reactor studied, j_{ORR} was determined by the electrolyte concentration regulating O_2 transport to the catalyst. This insight into the local operando gas diffusion rate, electrolyte concentration, and reaction rate would also be able to help determine if water activity becomes a dominant factor in other types of reactors, such as those for CO_2R. It thus serves as a strong model for future work on other electrocatalytic systems to better understand the local environment of CO_2R in GDEs operating at high current densities.

Experiment and Modeling Needs of CO_2R. To our knowledge, the careful comparison of experimental and modeling results of electrode dynamics has not yet been reported for CO_2R to the extent discussed above for ORR. Likewise, well-controlled studies such as that with the ORR at a nanopipette,[25] which singled out the effect of water activity on the ORR, could provide useful information about CO_2R. This could aid future modeling efforts that attempt to account for variations in water and solute activity. These insights can guide understanding of the diverse multiphase chemistry associated with CO_2R: carbonate and bicarbonate equilibria,[57,58] CO_2 consumption by hydroxide, and multiple simultaneous product activities. These added complexities are absent in ORR, so explicit CO_2 centric studies would be needed.

Expanding briefly on the bicarbonate and carbonate equilibria present for CO_2R, we point out that acid−base reactions depend on activities just as electrochemical reactions do. So, for 5−7 M NaOH or KOH, which have OH^- activity coefficient much greater than 1 and water activity below 1, the rate of conversion of CO_2 to (bi)carbonate will be faster than predicted by approximate calculations that replace activities with concentrations. The relevant reactions as typically written are[59]

$$CO_2 + H_2O \rightleftarrows HCO_3^- + H^+, \quad pKa_{18} = 6.35\ (25\ ^\circ C) \tag{18}$$

https://doi.org/10.1021/acs.jpcc.1c01923
J. Phys. Chem. C XXXX, XXX, XXX−XXX

Pursuant to the DOE Public Access Plan, this document represents the authors' peer-reviewed, accepted manuscript.
The published version of the article is available from the relevant publisher.

$$HCO_3^- \rightleftarrows CO_3^{2-} + H^+, \quad pKa_{19} = 10.33\ (25\ ^\circ C) \tag{19}$$

where Ka_{18} and Ka_{19} are the equilibrium constants of reactions 18 and 19, respectively. Simultaneously, similar reactions can occur directly with OH^-; as discussed in the literature, these occur at an appreciable rate only at pH greater than 6,[60−62]

$$CO_2 + OH^- \rightleftarrows HCO_3^- \tag{20}$$

$$HCO_3^- + OH^- \rightleftarrows CO_3^{2-} + H_2O \tag{21}$$

Further work on the Tafel slope and the reaction order of various species in CO_2R on GDEs would offer increased clarity on how to improve reaction activity and energy efficiency. The latter is maximized if current is kept below the mass transport limited regime (i.e., in the kinetically limited regime), undesired side reactions are avoided, and kinetics are optimized by a low Tafel slope and high exchange current density. Compared to solid electrodes, GDEs have improved mass transport of CO_2 to allow ∼1 A cm^{-2} COER and have allowed use of concentrated KOH electrolytes that improved electrolyte ionic conductivity and suppressed HER.[3,4,39] To optimize performance, it should be ensured these improvements did not come at the cost of increased Tafel slope or lowered exchange current density. Tafel slopes are lowest when the RDS is near the end of the reaction steps. An RDS near the end of the reaction steps also causes the exchange current density (via the rate expression) to be positively correlated to reactant concentration and negatively correlated to product concentration, e.g. rate expressions in eqs 15 and 16.

Little work has been done to measure Tafel slope or exchange current density of CO_2R at GDEs for different electrolytes. One study of Cu GDEs showed increasing exchange current density and a slightly decreasing Tafel slope for increasing $KHCO_3$ and KOH concentration (up to 1 M $KHCO_3$ and 2 M KOH).[63] This trend is opposite that suggested in eqs 15 or 16. When combined with the reported Tafel slope being 74−95 mV dec^{-1}, this trend suggests the GDE RDS was an early step, either CO_2 binding or the first protonation. For comparison, solid nanostructured electrodes have demonstrated Tafel slopes of 60 mV dec^{-1} on Ag[35] and 40 mV dec^{-1} on Au,[64−66] which correlate with the RDS as the final step before release of the CO.

These solid nanostructured electrodes also showed high selectivity for COER over HER in comparison to planar electrodes. Limiting water supply to a planar solid electrode was recently demonstrated as another avenue to the high selectivity: a solid planar Au electrode in a water-in-salt electrolyte lowered water concentration and improved selectivity for COER over HER.[67] However, the Tafel slope was ∼122−129 mV dec^{-1}, correlating to the first electron transfer to CO_2.

While GDEs have allowed increased CO_2 supply and lowered H_2O concentration (via hydroxide electrolytes), the water-in-salt electrolyte lowered H_2O concentration for a constant CO_2 supply. Both have achieved high selectivity for COER by increasing the concentration ratio of CO_2 to H_2O, but also reported high Tafel slopes. Nanostructured catalysts with sufficient CO_2 and H_2O, on the other hand, have shown high selectivity for COER with low Tafel slope. This suggests optimization of CO_2R GDEs may come from improved catalysts and increased water supply (commensurate with the plentiful CO_2 available to the GDE). More information on Tafel slopes and reactant and product reaction orders of CO_2R GDEs are needed to confirm or refute this projection.

It is relevant to compare the aforementioned analysis on water management and alkaline electrolytes to recent work that has used concentrated KOH (5−7 M) to report record CO_2R current densities as high as 1 A cm^{-2}.[4] From the perspective of this article, the high current density with favorable selectivity for CO_2R over HER can be understood in the following manner. The ionic conductivity of KOH is maximized at 7 M, with lower concentrations limited by ion concentration and higher concentrations limited by viscosity.[20] Thus, the potential drop in the cell from ohmic losses, which can be large at a high current density like 1 A cm^{-2}, was minimized by using 5−7 M KOH. Regarding selectivity for CO_2R over HER, in comparison to H-cell reactors with neutral pH bulk electrolytes, the concentrated hydroxide maintains very low proton concentration while the GDE provides a large supply of CO_2; together, these conditions favor CO_2R over HER, and the cell potential can be increased as needed to achieve high current densities without a CO_2 mass transport limitation. However, the take-away message of this article is that a low water supply and high hydroxide concentration will cause the first reaction step, CO_2 binding to the catalyst, to be the RDS. If a sufficiently high supply of water and low concentration of hydroxide were provided, the RDS may be later in the reaction mechanism series of steps, which would provide a lower Tafel slope for the cathode and improved energy efficiency of the cell.

Computational modeling has demonstrated that the local pH can go above 14 and the K^+ molarity go above 10 M at high CO_2R current densities, even for neutral pH bulk electrolytes, such as 0.5 M $KHCO_3$.[1,8,19,37] In addition, water films of ∼3 nm or less, which may be present in a GDE at the gas−liquid interface, have been predicted to have low water activity.[68] However, models of liquid electrolytes do not use activity-dependent reaction rates. These assumptions likely ignore important variations in reaction rate and equilibrium potentials throughout the CL, and thus, they cannot give a complete picture of the local reaction environment.

One example of a possible improvement from accounting for water and solute activity is the following: instead of needing artificial boundary conditions to capture the drop-off to zero of CO_2R current at the gas−liquid interface, as is typically done, inclusion of the water and solute activity effect on reaction rate may naturally produce this drop-off. Overall, including water and solute activity should provide more realistic insights into the current distribution and selectivity of GDEs for CO_2R.

CONCLUSIONS

In conclusion, water supply in a GDE CL will control CO_2R in many important ways. The local electrolyte concentration, which is driven upward by CO_2R, increases viscosity, slows diffusion, lowers conductivity of NaOH and KOH over 5−7 M, lowers CO_2 solubility, increases the conversion rate of CO_2 to (bi)carbonate, increases the solute activity coefficient, and lowers the water activity. The lowered water activity and increased solute activity should slow the COER rate and shift reaction equilibrium potentials. However, these effects have received little attention in experimental or modeling studies. Since these effects may become increasingly important as CO_2R devices are pushed toward current densities above 1 A cm^{-2}, here we have detailed the likely role of water and solute activities in CO_2R and surveyed work from relevant adjacent research fields to indicate what experimental and modeling work could provide a better understanding of CO_2R.

https://doi.org/10.1021/acs.jpcc.1c01923
J. Phys. Chem. C XXXX, XXX, XXX−XXX

Pursuant to the DOE Public Access Plan, this document represents the authors' peer-reviewed, accepted manuscript.
The published version of the article is available from the relevant publisher.

■ ASSOCIATED CONTENT

Supporting Information

The Supporting Information is available free of charge at https://pubs.acs.org/doi/10.1021/acs.jpcc.1c01923.

Appendix A:, approximation of CO activity at 298 K; Appendix B, dependence of equilibrium potential on log−log concentration vs activity plots; Appendix C, polynomial fits of KOH and NaOH water and solute activity; Appendix D, derivation of standard potential for acidic vs alkaline electrolytes; Appendix E, summary of ORR dependence on reactant activity; Appendix F, additional plots on activities and their effects; Appendix G, derivation of Nernst equation; and Appendix H, additional plots from 1D model(PDF)

■ AUTHOR INFORMATION

Corresponding Authors

Nathan T. Nesbitt − *Materials, Chemical, and Computational Science (MCCS) Directorate, National Renewable Energy Laboratory, Golden, Colorado 80401, United States;* orcid.org/0000-0002-1806-1077; Email: nathan.nesbitt@nrel.gov

Wilson A. Smith − *Materials, Chemical, and Computational Science (MCCS) Directorate, National Renewable Energy Laboratory, Golden, Colorado 80401, United States; Department of Chemical and Biological Engineering and Renewable and Sustainable Energy Institute (RASEI), University of Colorado Boulder, Boulder, Colorado 80303, United States;* orcid.org/0000-0001-7757-5281; Email: wilson.smith@nrel.gov

Complete contact information is available at: https://pubs.acs.org/10.1021/acs.jpcc.1c01923

Author Contributions

N.T.N. and W.A.S. conceptualized the idea of the study and wrote the manuscript. N.T.N. ran the formal analysis and modeling.

Notes

Submitted to ChemRxiv: 15th January 2021. https://doi.org/10.26434/chemrxiv.13571141

The authors declare no competing financial interest.

Biographies

Nathan Nesbitt is a postdoctoral researcher in the Chemistry and Nanoscience Center at the National Renewable Energy Laboratory (NREL). He earned his BS in Physics from Worcester Polytechnic Institute in 2011 and his Ph.D. in Physics from Boston College in 2018, where he developed nanostructured electrodes for plasmonics and electrochemistry. In 2018 he moved to Delft, The Netherlands, as a postdoctoral researcher in Chemical Engineering at Delft University of Technology where he studied electrochemical CO_2 reduction at high current densities with operando microscopy. He has received fellowships from the Environmental Protection Agency and the National Science Foundation for research in renewable energy technology. He was on the Massachusetts Envirothon Council from 2014 to 2018 to support science and environmental advocacy among high school students, and his current diversity, equity, and inclusion efforts focus on youth intern programs in STEM. Nathan's current research interests are fundamentals of electrochemistry and operando microscopy of energy storage technology to facilitate equitable and sustainable energy infrastructure.

Wilson A. Smith is an Associate Professor in the Department of Chemical and Biological Engineering and the Renewable and Sustainable Energy Institute (RASEI) at University of Colorado Boulder. He earned his BS in Physics from American University in 2005 and his Ph.D. in Physics from the University of Georgia in 2010, where he studied the synthesis and applications of nanostructured photocatalysts. From there he moved to Paris, France, as a postdoctoral research associate at the Universite Pierre et Marie Curie/Sorbonne where he studied the defect structure of doped semiconductors for solar water purification. In 2012 he began his independent career at TU Delft, where his group focused on fundamental and applied aspects of photoelectrochemical water splitting, electrochemical CO_2 reduction and ammonia synthesis. In 2019 he took a joint appointment at the University of Colorado Boulder and the National Renewable Energy Lab. Wilson has been the recipient of the prestigious VENI (2013), VIDI (2016), and ERC (2017) personal grants, which have helped his group bridge scales and disciplines to address practical problems in large scale energy conversion and storage.

■ ACKNOWLEDGMENTS

This material on homogeneous reaction effects is based on work performed by the Liquid Sunlight Alliance, which is supported by the U.S. Department of Energy, Office of Science, Office of Basic Energy Sciences, Fuels from Sunlight Hub, under Award Number DE-SC0021266. This work was authored in part by the National Renewable Energy Laboratory (NREL), operated by the Alliance for Sustainable Energy, LLC, for the U.S. Department of Energy (DOE) under Contract No. DE-AC36-08GO28308. This work on reaction modeling and effects on heterogeneous reactions was supported by the Laboratory Directed Research and Development (LDRD) Program at NREL. The views expressed in the article do not necessarily represent the views of the DOE or the U.S. Government. The U.S. Government retains and the publisher, by accepting the

https://doi.org/10.1021/acs.jpcc.1c01923
J. Phys. Chem. C XXXX, XXX, XXX−XXX

Pursuant to the DOE Public Access Plan, this document represents the authors' peer-reviewed, accepted manuscript.
The published version of the article is available from the relevant publisher.

article for publication, acknowledges that the U.S. Government retains a nonexclusive, paid-up, irrevocable, worldwide license to publish or reproduce the published form of this work, or allow others to do so, for U.S. Government purposes. The authors thank Recep Kas for fruitful discussions on fundamentals of electrochemistry.

REFERENCES

(1) Burdyny, T.; Smith, W. A. CO_2 Reduction on Gas-Diffusion Electrodes and Why Catalytic Performance Must Be Assessed at Commercially-Relevant Conditions. *Energy Environ. Sci.* **2019**, *12* (5), 1442−1453.
(2) Ma, S.; Sadakiyo, M.; Luo, R.; Heima, M.; Yamauchi, M.; Kenis, P. J. A. One-Step Electrosynthesis of Ethylene and Ethanol from CO_2 in an Alkaline Electrolyzer. *J. Power Sources* **2016**, *301*, 219−228.
(3) Jouny, M.; Luc, W.; Jiao, F. High-Rate Electroreduction of Carbon Monoxide to Multi-Carbon Products. *Nat. Catal.* **2018**, *1* (10), 748−755.
(4) García de Arquer, F. P.; Dinh, C.-T.; Ozden, A.; Wicks, J.; McCallum, C.; Kirmani, A. R.; Nam, D.-H.; Gabardo, C.; Seifitokaldani, A.; Wang, X.; et al. CO_2 Electrolysis to Multicarbon Products at Activities Greater than 1 Acm^{-2}. *Science* **2020**, *367* (6478), 661−666.
(5) Ma, W.; Xie, S.; Liu, T.; Fan, Q.; Ye, J.; Sun, F.; Jiang, Z.; Zhang, Q.; Cheng, J.; Wang, Y. Electrocatalytic Reduction of CO_2 to Ethylene and Ethanol through Hydrogen-Assisted C−C Coupling over Fluorine-Modified Copper. *Nat. Catal.* **2020**, *3*, 478−487.
(6) Chen, Y.; Vise, A.; Klein, W. E.; Cetinbas, F. C.; Myers, D. J.; Smith, W. A.; Deutsch, T. G.; Neyerlin, K. C. A Robust, Scalable Platform for the Electrochemical Conversion of CO_2 to Formate: Identifying Pathways to Higher Energy Efficiencies. *ACS Energy Lett.* **2020**, *5* (6), 1825−1833.
(7) Corral, D.; Feaster, J. T.; Sobhani, S.; DeOtte, J. R.; Lee, D. U.; Wong, A. A.; Hamilton, J.; Beck, V. A.; Sarkar, A.; Hahn, C.; et al. Advanced Manufacturing for Electrosynthesis of Fuels and Chemicals from CO 2. *Energy Environ. Sci.* **2021**, DOI: 10.1039/D0EE03679J.
(8) Weng, L.-C.; Bell, A. T.; Weber, A. Z. Modeling Gas-Diffusion Electrodes for CO_2 Reduction. *Phys. Chem. Chem. Phys.* **2018**, *20* (25), 16973−16984.
(9) Weng, L.-C.; Bell, A. T.; Weber, A. Z. Towards Membrane-Electrode Assembly Systems for CO_2 Reduction: A Modeling Study. *Energy Environ. Sci.* **2019**, *12* (6), 1950−1968.
(10) Delacourt, C.; Newman, J. Mathematical Modeling of CO_2 Reduction to CO in Aqueous Electrolytes: II. Study of an Electrolysis Cell Making Syngas from and Reduction at Room Temperature. *J. Electrochem. Soc.* **2010**, *157* (12), B1911.
(11) Wen, G.; Ren, B.; Gostick, J. T.; Chen, Z. Combined Simulation and Experimental Study of Electrolysis Flow Cell for Continuous CO_2 Conversion. *Meet. abstr. (Electrochem. Soc.)* **2020**, *MA2020-01* (36), 1503.
(12) Wu, K.; Birgersson, E.; Kim, B.; Kenis, P. J. A.; Karimi, I. A. Modeling and Experimental Validation of Electrochemical Reduction of CO_2 to CO in a Microfluidic Cell. *J. Electrochem. Soc.* **2015**, *162* (1), F23−F32.
(13) Chen, Y.; Xiang, C.; Lewis, N. Modeling the Performance of a Flow-Through Gas Diffusion Electrode for Electrochemical Reduction of CO or CO_2. *J. Electrochem. Soc.* **2020**, *167*, 114503.
(14) Brée, L. C.; Wessling, M.; Mitsos, A. Modular Modeling of Electrochemical Reactors: Comparison of CO_2-Electolyzers. *Comput. Chem. Eng.* **2020**, *139*, 106890.
(15) Georgopoulou, C.; Jain, S.; Agarwal, A.; Rode, E.; Dimopoulos, G.; Sridhar, N.; Kakalis, N. On the Modelling of Multidisciplinary Electrochemical Systems with Application on the Electrochemical Conversion of CO_2 to Formate/Formic Acid. *Comput. Chem. Eng.* **2016**, *93*, 160−170.
(16) Weng, L.-C.; Bell, A. T.; Weber, A. Z. A Systematic Analysis of Cu-Based Membrane-Electrode Assemblies for CO_2 Reduction through Multiphysics Simulation. *Energy Environ. Sci.* **2020**, *13* (10), 3592−3606.
(17) Reyes, A.; Jansonius, R. P.; Mowbray, B. A. W.; Cao, Y.; Wheeler, D. G.; Chau, J.; Dvorak, D. J.; Berlinguette, C. P. Managing Hydration at the Cathode Enables Efficient CO_2 Electrolysis at Commercially Relevant Current Densities. *ACS Energy Lett.* **2020**, *5*, 1612−1618.
(18) Nwabara, U. O.; de Heer, M. P.; Cofell, E. R.; Verma, S.; Negro, E.; Kenis, P. J. A. Towards Accelerated Durability Testing Protocols for CO_2 Electrolysis. *J. Mater. Chem. A* **2020**, *8* (43), 22557−22571.
(19) Zhang, F.; Co, A. C. Direct Evidence of Local PH Change and the Role of Alkali Cation during CO_2 Electroreduction in Aqueous Media. *Angew. Chem., Int. Ed.* **2020**, *59* (4), 1674−1681.
(20) Woo, A. L.-W. *Conductance Studies of Concentrated Solutions of Sodium Hydroxide and Potassium Hydroxide Electrolytes*; South Dakota State University: 1968; p 39.
(21) Ma, M.; Clark, E. L.; Therkildsen, K. T.; Dalsgaard, S.; Chorkendorff, I.; Seger, B. Insights into the Carbon Balance for CO_2 Electroreduction on Cu Using Gas Diffusion Electrode Reactor Designs. *Energy Environ. Sci.* **2020**, *13* (3), 977−985.
(22) Rabinowitz, J. A.; Kanan, M. W. The Future of Low-Temperature Carbon Dioxide Electrolysis Depends on Solving One Basic Problem. *Nat. Commun.* **2020**, *11* (1), 5231.
(23) Kas, R.; Star, A. G.; Yang, K.; Van Cleve, T.; Neyerlin, K. C.; Smith, W. A. Along the Channel Gradients Impacts on the Spatioactivity of Gas Diffusion Electrodes at High Conversions during CO_2 Electroreduction. *ACS Sustainable Chem. Eng.* **2021**, *9*, 1286−1296.
(24) Botz, A.; Clausmeyer, J.; Ohl, D.; Tarnev, T.; Franzen, D.; Turek, T.; Schuhmann, W. Local Activities of Hydroxide and Water Determine the Operation of Silver-Based Oxygen Depolarized Cathodes. *Angew. Chem., Int. Ed.* **2018**, *57* (38), 12285−12289.
(25) Clausmeyer, J.; Botz, A.; Ohl, D.; Schuhmann, W. The Oxygen Reduction Reaction at the Three-Phase Boundary: Nanoelectrodes Modified with Ag Nanoclusters. *Faraday Discuss.* **2016**, *193* (0), 241−250.
(26) Röhe, M.; Botz, A.; Franzen, D.; Kubannek, F.; Ellendorff, B.; Ohl, D.; Schuhmann, W.; Turek, T.; Krewer, U. The Key Role of Water Activity for the Operating Behavior and Dynamics of Oxygen Depolarized Cathodes. *ChemElectroChem* **2019**, *6* (22), 5671−5681.
(27) Akerlof, G. C.; Bender, P. Thermodynamics of Aqueous Solutions of Potassium Hydroxide. *J. Am. Chem. Soc.* **1948**, *70* (7), 2366−2369.
(28) Åkerlöf, G.; Kegeles, G. Thermodynamics of Concentrated Aqueous Solutions of Sodium Hydroxide. *J. Am. Chem. Soc.* **1940**, *62* (3), 620−640.
(29) Sipos, P. M.; Hefter, G.; May, P. M. Viscosities and Densities of Highly Concentrated Aqueous MOH Solutions (M^+ = Na^+, K^+, Li^+, Cs^+, $(CH_3)_4N^+$) at 25.0 °C. *J. Chem. Eng. Data* **2000**, *45* (4), 613−617.
(30) Balej, J. Water Vapour Partial Pressures and Water Activities in Potassium and Sodium Hydroxide Solutions over Wide Concentration and Temperature Ranges. *Int. J. Hydrogen Energy* **1985**, *10* (4), 233−243.
(31) Pérez-Villasenor, F.; Iglesias-Silva, G. A.; Hall, K. R. Osmotic and Activity Coefficients Using a Modified Pitzer Equation for Strong Electrolytes 1:1 and 1:2 at 298.15 K. *Ind. Eng. Chem. Res.* **2002**, *41* (5), 1031−1037.
(32) Lewis, G. N.; Randall, M. The Activity Coefficient of Strong Electrolytes. *J. Am. Chem. Soc.* **1921**, *43*, 1112−1153.
(33) Debye, P.; Huckel, E. Zur Theory Der Elektrolyte. *Phys. Z.* **1923**, *24*, 185.
(34) Pitzer, K. S. Thermodynamics of Electrolytes. I. Theoretical Basis and General Equations. *J. Phys. Chem.* **1973**, *77* (2), 268−277.
(35) Rosen, J.; Hutchings, G. S.; Lu, Q.; Rivera, S.; Zhou, Y.; Vlachos, D. G.; Jiao, F. Mechanistic Insights into the Electrochemical Reduction of CO_2 to CO on Nanostructured Ag Surfaces. *ACS Catal.* **2015**, *5* (7), 4293−4299.
(36) Ooka, H.; Figueiredo, M. C.; Koper, M. T. M. Competition between Hydrogen Evolution and Carbon Dioxide Reduction on Copper Electrodes in Mildly Acidic Media. *Langmuir* **2017**, *33* (37), 9307−9313.

https://doi.org/10.1021/acs.jpcc.1c01923
J. Phys. Chem. C XXXX, XXX, XXX−XXX

Pursuant to the DOE Public Access Plan, this document represents the authors' peer-reviewed, accepted manuscript.
The published version of the article is available from the relevant publisher.

(37) Yang, K.; Kas, R.; Smith, W. A. In Situ Infrared Spectroscopy Reveals Persistent Alkalinity near Electrode Surfaces during CO_2 Electroreduction. *J. Am. Chem. Soc.* **2019**, *141* (40), 15891−15900.
(38) Wuttig, A.; Yoon, Y.; Ryu, J.; Surendranath, Y. Bicarbonate Is Not a General Acid in Au-Catalyzed CO_2 Electroreduction. *J. Am. Chem. Soc.* **2017**, *139* (47), 17109−17113.
(39) Dinh, C.-T.; Burdyny, T.; Kibria, M. G.; Seifitokaldani, A.; Gabardo, C. M.; García de Arquer, F. P.; Kiani, A.; Edwards, J. P.; De Luna, P.; Bushuyev, O. S.; et al. CO_2 Electroreduction to Ethylene via Hydroxide-Mediated Copper Catalysis at an Abrupt Interface. *Science* **2018**, *360* (6390), 783−787.
(40) Diamond, L. W.; Akinfiev, N. N. Solubility of CO_2 in Water from − 1.5 to 100 °C and from 0.1 to 100 MPa: Evaluation of Literature Data and Thermodynamic Modelling. *Fluid Phase Equilib.* **2003**, *208* (1), 265−290.
(41) Sander, R. Compilation of Henry's Law Constants (Version 4.0) for Water as Solvent. *Atmos. Chem. Phys.* **2015**, *15* (8), 4399−4981.
(42) Meadows, R. W.; Spedding, D. J. The Solubility of Very Low Concentrations of Carbon Monoxide in Aqueous Solution. *Tellus* **1974**, *26* (1−2), 143−150.
(43) Dake, S. B.; Chaudhari, R. V. Solubility of Carbon Monoxide in Aqueous Mixtures of Methanol, Acetic Acid, Ethanol and Propionic Acid. *J. Chem. Eng. Data* **1985**, *30* (4), 400−403.
(44) Douglas, E. Carbon Monoxide Solubilities in Sea Water. *J. Phys. Chem.* **1967**, *71* (6), 1931−1933.
(45) Khan, M. M. T.; Halligudi, S. B. Solubility of Carbon Monoxide in Aqueous Mixtures of Allyl Alcohol, Diethylamine, and Triethylamine. *J. Chem. Eng. Data* **1988**, *33* (3), 276−278.
(46) Chapter 9: Mixtures https://chem.libretexts.org/Bookshelves/Physical_and_Theoretical_Chemistry_Textbook_Maps/DeVoes_Thermodynamics_and_Chemistry/09%3A_Mixtures (accessed Nov 6, 2020).
(47) Weekes, D. M.; Salvatore, D. A.; Reyes, A.; Huang, A.; Berlinguette, C. P. Electrolytic CO_2 Reduction in a Flow Cell. *Acc. Chem. Res.* **2018**, *51* (4), 910−918.
(48) Li, Y. C.; Zhou, D.; Yan, Z.; Goncalves, R. H.; Salvatore, D. A.; Berlinguette, C. P.; Mallouk, T. E. Electrolysis of CO_2 to Syngas in Bipolar Membrane-Based Electrochemical Cells. *ACS Energy Lett.* **2016**, *1* (6), 1149−1153.
(49) Salvatore, D.; Berlinguette, C. P. Voltage Matters When Reducing CO_2 in an Electrochemical Flow Cell. *ACS Energy Lett.* **2020**, *5* (1), 215−220.
(50) Salvatore, D. A.; Weekes, D. M.; He, J.; Dettelbach, K. E.; Li, Y. C.; Mallouk, T. E.; Berlinguette, C. P. Electrolysis of Gaseous CO_2 to CO in a Flow Cell with a Bipolar Membrane. *ACS Energy Lett.* **2018**, *3* (1), 149−154.
(51) Li, X.; Sabir, I. Review of Bipolar Plates in PEM Fuel Cells: Flow-Field Designs. *Int. J. Hydrogen Energy* **2005**, *30* (4), 359−371.
(52) Cleghorn, S. J. C.; Derouin, C. R.; Wilson, M. S.; Gottesfeld, S. A Printed Circuit Board Approach to Measuring Current Distribution in a Fuel Cell. *J. Appl. Electrochem.* **1998**, *28* (7), 663−672.
(53) Osmieri, L.; Mauger, S.; Ulsh, M.; Neyerlin, K. C.; Bender, G. Use of a Segmented Cell for the Combinatorial Development of Platinum Group Metal-Free Electrodes for Polymer Electrolyte Fuel Cells. *J. Power Sources* **2020**, *452*, 227829.
(54) Wang, X.; de Araujo, J. F.; Ju, W.; Bagger, A.; Schmies, H.; Kuhl, S.; Rossmeisl, J.; Strasser, P. Mechanistic Reaction Pathways of Enhanced Ethylene Yields during Electroreduction of CO_2−CO Co-Feeds on Cu and Cu-Tandem Electrocatalysts. *Nat. Nanotechnol.* **2019**, *14* (11), 1063−1070.
(55) Yang, H.-H.; McCreery, R. L. Elucidation of the Mechanism of Dioxygen Reduction on Metal-Free Carbon Electrodes. *J. Electrochem. Soc.* **2000**, *147*, 3420.
(56) Zhang, C.; Fan, F.-R. F.; Bard, A. J. Electrochemistry of Oxygen in Concentrated NaOH Solutions: Solubility, Diffusion Coefficients, and Superoxide Formation. *J. Am. Chem. Soc.* **2009**, *131* (1), 177−181.
(57) Han, X.; Yu, Z.; Qu, J.; Qi, T.; Guo, W.; Zhang, G. Measurement and Correlation of Solubility Data for CO_2 in $NaHCO_3$ Aqueous Solution. *J. Chem. Eng. Data* **2011**, *56* (4), 1213−1219.
(58) Hitchcock, L. B. Rate of Absorption of Carbon Dioxide Effect of Concentration and Viscosity of Caustic Solutions. *Ind. Eng. Chem.* **1934**, *26* (11), 1158−1167.
(59) Hori, Y.; Vayenas, C. G.; White, R. E.; Gamboa-Aldeco, M. E. Electrochemical CO_2 Reduction on Metal Electrodes. *Modern Aspects of Electrochemistry* **2008**, *42*, 89−189.
(60) Himmelblau, D. M.; Babb, A. L. Kinetic Studies of Carbonation Reactions Using Radioactive Tracers. *AIChE J.* **1958**, *4* (2), 143−152.
(61) Pohorecki, R.; Moniuk, W. Kinetics of Reaction between Carbon Dioxide and Hydroxyl Ions in Aqueous Electrolyte Solutions. *Chem. Eng. Sci.* **1988**, *43* (7), 1677−1684.
(62) Hikita, H.; Asai, S.; Takatsuka, T. Absorption of Carbon Dioxide into Aqueous Sodium Hydroxide and Sodium Carbonate-Bicarbonate Solutions. *Chem. Eng. J.* **1976**, *11* (2), 131−141.
(63) Xiang, H.; Rasul, S.; Scott, K.; Portoles, J.; Cumpson, P.; Yu, E. H. Enhanced Selectivity of Carbonaceous Products from Electrochemical Reduction of CO_2 in Aqueous Media. *J. CO2 Util.* **2019**, *30*, 214−221.
(64) Nesbitt, N. T.; Ma, M.; Trzesniewski, B. J.; Jaszewski, S.; Tafti, F.; Burns, M. J.; Smith, W. A.; Naughton, M. J. Au Dendrite Electrocatalysts for CO_2 Electrolysis. *J. Phys. Chem. C* **2018**, *122* (18), 10006−10016.
(65) Saberi Safaei, T.; Mepham, A.; Zheng, X.; Pang, Y.; Dinh, C.-T.; Liu, M.; Sinton, D.; Kelley, S. O.; Sargent, E. H. High-Density Nanosharp Microstructures Enable Efficient CO_2 Electroreduction. *Nano Lett.* **2016**, *16* (11), 7224−7228.
(66) Ringe, S.; Morales-Guio, C. G.; Chen, L. D.; Fields, M.; Jaramillo, T. F.; Hahn, C.; Chan, K. Double Layer Charging Driven Carbon Dioxide Adsorption Limits the Rate of Electrochemical Carbon Dioxide Reduction on Gold. *Nat. Commun.* **2020**, *11* (1), 33.
(67) Dong, Q.; Zhang, X.; He, D.; Lang, C.; Wang, D. Role of H_2O in CO_2 Electrochemical Reduction as Studied in a Water-in-Salt System. *ACS Cent. Sci.* **2019**, *5* (8), 1461−1467.
(68) Bockris, J. O.'M.; Cahan, B. D. Effect of a Finite-Contact-Angle Meniscus on Kinetics in Porous Electrode Systems. *J. Chem. Phys.* **1969**, *50* (3), 1307−1324.

https://doi.org/10.1021/acs.jpcc.1c01923
J. Phys. Chem. C XXXX, XXX, XXX−XXX